Laser-ion accelerators: State-of-the-art and scaling laws

Laser-ion accelerators: State-of-the-art and scaling laws

M. Borghesi, S. Kar, and D. Margarone

Citation: AIP Conf. Proc. **1546**, 3 (2013); doi: 10.1063/1.4816600
View online: http://dx.doi.org/10.1063/1.4816600
View Table of Contents: http://proceedings.aip.org/dbt/dbt.jsp?KEY=APCPCS&Volume=1546&Issue=1
Published by the AIP Publishing LLC.

Laser-ion accelerators: state-of-the-art and scaling laws

M. Borghesi [a,b], S. Kar [a], D. Margarone[b]

[a] *Centre for Plasma Physics, Queen's University Belfast, Belfast BT7 1NN, UK*
[b]*Institute of Physics of the ASCR, ELI-Beamlines Project, Prague, Czech Republic*

Abstract. A significant amount of experimental work has been devoted over the last decade to the development and optimization of proton acceleration based on the so-called Target Normal Sheath acceleration mechanism. Several studies have been dedicated to the determination of scaling laws for the maximum energy of the protons as a function of the parameters of the irradiating pulses, studies based on experimental results and on models of the acceleration process. We briefly summarize the state of the art in this area, and review some of the scaling studies presented in the literature. We also discuss some recent results, and projected scalings, related to a different acceleration mechanism for ions, based on the Radiation Pressure of an ultraintense laser pulse.

INTRODUCTION

Several foreseen applications of laser driven ion beams require a substantial increase of the energy per nucleon beyond 100 MeV. Up to now, the maximum energy of protons accelerated from solid targets in the TNSA (target normal sheath acceleration) regime is 67.5 MeV [1]. This energy was achieved for special flat top hollow micro-cone target at Trident laser, while the highest energies obtained in TNSA from flat foils are of the order of 60 MeV (obtained on the Nova [2] and VULCAN Petawatt [3] systems). Highest energies reported for ultra-short laser pulses (10s of fs, on the JKaren laser) are of the order of 40 MeV [4]; there are reports of yet unpublished results showing higher energies (120 MeV protons and carbon ions with 80 MeV per nucleon) obtained in the Break Out Afterburner regime at the Trident laser, Los Alamos National Laboratory [5].

In comparing all these values, one should however exert some caution, as the highest energies reported may not necessarily correspond to an effective cut-off energy, but may be determined instead by the energy at which the spectral signal decreases below the instrumental detection threshold, which varies depending on the details of the diagnostic employed. Currently the laser intensities available on target are a limiting factor on the maximum achievable ion energy. While intensities of the order of 10^{22} W/cm^2 [4] have been reported, in practice the maximum on-target intensities achieved in experiments so far are ~ 10^{21} W/cm^2 (e.g. [3-4], [6]). A next generation of laser facilities will allow higher intensities than this value, hence paving the way towards higher ion energies. In this respect it is of crucial importance to establish the most relevant scaling laws, which can anticipate the future achievable laser driven ion energies.

Nevertheless, there are other ion beam parameters, which are of relevance and need to be improved or controlled for specific applications. For instance, TNSA proton beams are highly laminar and have very low emittance [7], but their divergence is a concern for application requiring proton transport to a secondary target; TNSA energy spectra are ordinarily broad and thus unsuitable for direct use in many applicative contexts; furthermore, for most applications, including cancer therapy, the requirement of reaching sufficiently high energies is coupled to the need of having a sufficiently large number of particles in the energy range under consideration. These issues motivate scientists to search for new ion acceleration mechanisms such as Radiation Pressure Acceleration (RPA) and Collisionless Shock Acceleration (CSA). Other proposed schemes exploit the potential both of advanced target engineering and of nonlinear-relativistic optical effects in plasmas, such as ion acceleration in ultrathin solid targets which become transparent to intense laser pulses (Break-Out Afterburner, BOA) or involving low density targets (see [8] for a review of all these emerging mechanisms). However, the understanding, and experimental implementation, of the fundamental processes governing these mechanisms are still under development.

EXPERIMENTAL SCALING LAWS FOR TNSA

An analysis of TNSA proton acceleration experiments suggests a scaling of $(I\lambda^2)^{1/2}$ for the proton maximum energy, where I is the laser intensity and λ the laser wavelength, which is valid up to values of $I\lambda^2=3x10^{20}$ Wcm$^-$

2nd ELIMED Workshop and Panel
AIP Conf. Proc. 1546, 3-8 (2013); doi: 10.1063/1.4816600

$^2\mu m^2$ [7]. Fig.1 summarizes data obtained up to 2008 [9], together with some more recent results (green points) obtained with ultrashort (tens fs) pulses . The maximum proton energy is reported as a function of the laser irradiance and for three different ranges of pulse durations. Two trend lines are overlayed, the shallower one corresponding to $(I\lambda^2)^{1/2}$ dependence, and the steeper one indicating a scaling law proportional to $I\lambda^2$. In [3] it is suggested that the observed $(I\lambda^2)^{1/2}$ scaling, if maintained at higher intensities, would lead to 200 MeV cut-off energies (at the high end of the range of relevance for cancer therapy) at intensities of the order of 5 10^{21} W/cm^2.

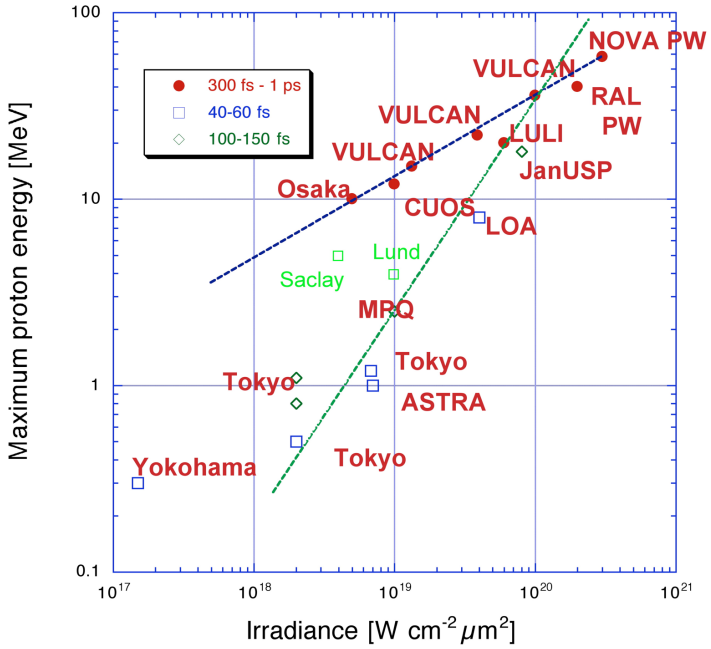

FIGURE 1. Maximum proton energy from laser-irradiated solid targets as a function of the laser irradiance and for three ranges of pulse durations (see [7] for detailed references) , with additional data (labels "Lund" and "Saclay") reporting later experiments up to 2008. Two trend lines are overlaid, the shallower one corresponding to a $I^{1/2}$ dependence, and the steeper one to a scaling proportional to I. Reprinted from [9]

.

However, it is clear that the irradiance is not the only laser parameter playing a role in determining the maximum laser-accelerated ion energy. Fig.1 already shows that, for the same irradiance, more energetic pulses lead to higher maximum energies. Furthermore, several secondary factors (e.g., such as prepulse energy and duration, target thickness) also affect the maximum energy measurable. Several other parametric investigations of the dependence of E_{max} on laser pulse irradiance, duration, energy and fluence have been reported (e.g. [3,6, 12]). Fig. 2 shows results from one such parametric study of the dependence of the maximum proton energy on laser power and duration, carried out on a single laser facility [6], showing a quasi-linear dependence on laser energy.

Two main classes of approaches have been developed to describe analytically this process with the aim of matching current results and predict what will happen at higher intensities. A first approach considers ions and hot electrons as an expanding plasma, and its expansion is described with fluid models [10-12] as an extension of the classical case of a plasma expanding into vacuum [13], driven by the ambipolar electric field generated in a narrow layer at the front of the plasma cloud. In this approach, the acceleration of the ions modifies the field and determines its evolution.

A simple approach based on an isothermal expansion leads to diverging ion energies, unless the acceleration time is constrained artificially, as done for example in [12], where it is shown that choosing a specific acceleration time leads to a good match between model predictions and experimental scalings. More realistic adiabatic models which account for the finite energy of the hot electrons have also been developed [13].

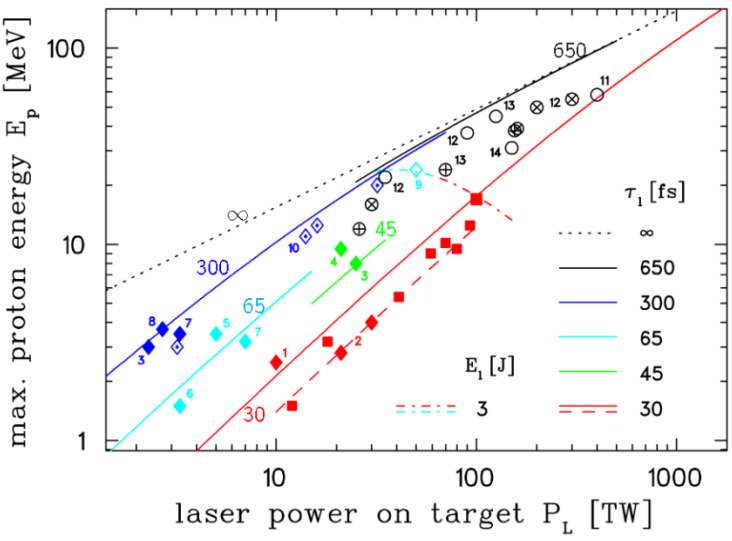

FIGURE 2. Experimental scaling of proton energy cutoff with laser power and pulse duration. Squares are data from experiments performed with the DRACO laser at FZD (Dresden), showing a linear scaling with power in the short-pulse (30 fs) regime. Other points are data from other laboratories; see [6] for references and details. The fitting lines correspond to the static model discussed in [14] with different colors (labels) corresponding to different values of the of the pulse duration τ_l as given in the legend.

A different approach assumes that the light ions, or at least the most energetic ones, are accelerated mostly in the early stage of the formation of the sheath, so that the sheath field may be assumed as almost stationary. In these conditions, the effects of the light ions on the electrostatic potential are usually neglected, while the heavy ion population is considered immobile. These models aim to provide the most accurate description of the sheath field depending on assumptions on the fast electron distributions. An expression for the potential φ created by thermal electrons extending beyond a sharp solid-vacuum interface was found by Crow et al [15]. The main issue is that the potential extends to infinity and leads to infinite ion acceleration, unless a spatial truncation of φ is introduced, as suggested in [16].

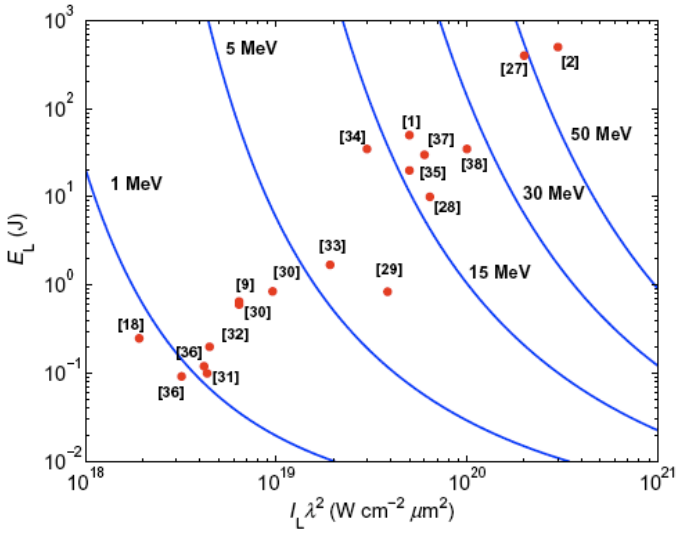

FIGURE 3. Curves of constant proton energy $\mathcal{E}_{\max}$ (in MeV) plotted in the $(I\lambda^2; E_L)$ plane (laser irradiance and energy), as derived from the model discussed in [16-17]. Ranges relevant for present facilities are considered. A collection of experimental maximum proton energies is superimposed (red dots). Details about the experimental conditions are contained in [17].

In this paper, only the contribution of electron trapped in the potential of a charged target is considered, which leads to a spatial limitation of the potential contributing to ion acceleration, and a model for the maximum ion energy as a function of laser parameters (energy and intensity). The maximum trapped electron energy is estimated from a semi-empirical approach by comparison with a set of experimental data. Scalings for the ion energy based on this model appear to match a large fraction of experimental results so far [17] (see fig. 3), and can be used as a predictive tool for future experiment. For example, this type of modeling predicts that cut-off energies of 200 MeV may be reached with irradiance approaching 10^{22} W cm^2 μm^{-2} and laser energies in the 10J region.

RECENT RESULTS AND SCALING LAWS TOWARDS THE RADIATION PRESSURE ACCELERATION REGIME

Radiation Pressure Acceleration (RPA) is currently attracting a substantial amount of experimental and theoretical attention due to the predicted superior scaling in terms of ion energy and laser-ion conversion efficiency. In this context, the so called 'Light Sail'(LS) [8] scheme, where, for a sufficiently thin foil, the whole laser-irradiated area is detached and pushed forward by the Radiation Pressure, is particularly promising.

Assuming the foil to be a perfect mirror of thickness d, its nonrelativistic motion may be simply described by $m_i n_i d\frac{dV}{dt}=\frac{2I}{c}$ from which we obtain an energy $\varepsilon_i = m_i\frac{V^2}{2}=\frac{2F^2}{m_i n_i^2 d^2 c^2}$ where $F=\int I\,dt$ $F=\int Idt$ is the laser pulse fluence. Assuming a temporally flat top pulse, one obtains a dependence $\varepsilon_i \approx \left(\frac{a_0^2\tau}{\chi}\right)^2$, i.e. a much stronger dependence on I than TNSA. $a_0 \sim \sqrt{I}$ is the dimensionless laser intensity, τ is the laser pulse duration and $\chi=(\rho/m_p n_c)(l/\lambda)$ is the normalised target areal density (ρ – target density; m_p – proton mass; n_c – critical plasma density; l – target thickness and λ – incident laser wavelength).

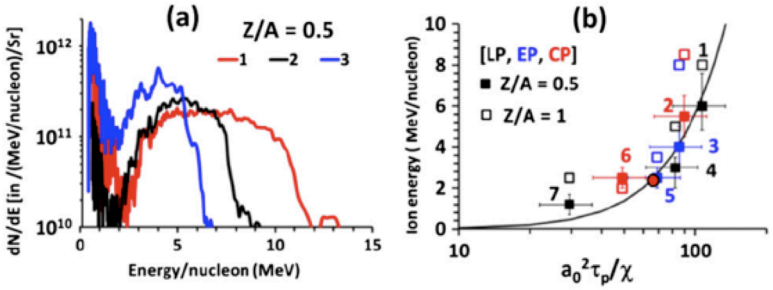

FIGURE 4. Three typical narrow-band spectra for Z/A= 1/2 impurity ions observed from thin (0:1 μm) metallic targets [17]. For parameters of shots 1–3, see the explanation in (b). (b) Peak energies for both ions with Z/A =1/2 (filled squares) and protons with Z/A=1 (empty squares) for seven shots with different polarization parameters ε = 0 (LP), 0.47 (EP), and 0.88 (CP). The peak energy is plotted as a function of the parameter $a_0^2\tau_p/\chi$ discussed earlier. The parameter set [a0, target material, thickness (μm), polarization] for the data points 1-7 is [15.5, Cu, 0.1, LP], [10, Cu, 0.05, CP], [13.8, Cu, 0.1, EP], [7.5, Al, 0.1, LP], [6.9, Al, 0.1, EP], [13.6, Al, 0.5, CP], and [14.1, Al, 0.8, LP], respectively. The solid line is the LS scaling.

For extremely thin (a few nm) targets, the breakthrough of the laser pulse through the foil due to relativistic transparency may stop LS-RPA, but at the same time lead to strong heating of electrons. This effect opens up a regime of possible enhanced acceleration (e.g. the BOA mechanism mentioned earlier).
The RPA-LS scheme for ion acceleration was extensively studied in a recent experiment carried out employing the PW arm of the VULCAN laser system at the Rutherford Appleton Laboratory, STFC, UK [18]. The laser delivered ~ 200 J energy on target in sub- ps pulses, focused on target at normal incidence by an f/3 off axis parabolic mirror, reaching peak intensity ~ 3×10^{20} W/cm^2. Targets of different composition and thickness were irradiated and the ion

spectra produced by the interaction were diagnosed by two Thomson parabola (TP) spectrometers and Radiochromic film (RCF) stacks.
Unlike exponential spectra observed from 5-10 μm thick foil targets, narrow-band features in proton and heavier ion spectra were obtained from sub-μm thick targets irradiated at high intensities (for an example of Carbon spectra, see Fig. 4(a)).

The peaks observed in the carbon spectra along the laser axis were not observed in the off-axis detector TP2, indicating that they are confined within a cone of half-aperture less than 13 ± 2 deg (the view angle of the off axis TP).

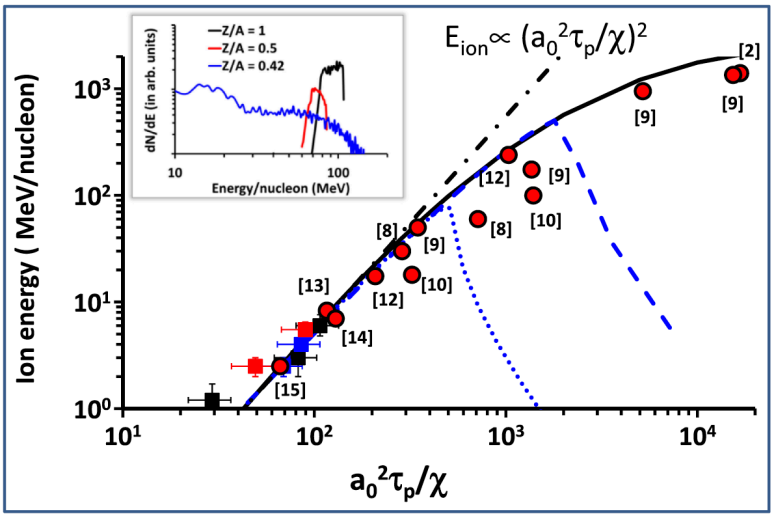

FIGURE 5. Ion energy scaling (solid, black line) as shown in Fig. 2(b), extrapolated to higher $a_0^2\tau_p/\chi$, and assuming target reflectivity equal to 1. Square points are the experimental data shown in the same figure. The (red) circles represent the spectral peaks reported in the literature, as labeled, from multispecies PIC simulations for stable LS acceleration (see [17] for a list of references). The dot-dashed (black) line shows the $\left(a_0^2\tau_p/\chi\right)^2$ scaling valid for nonrelativistic ion energies. Dotted and dashed (blue) lines show the ion energy trend predicted by the rigid model by varying c for 45 fs FWHM laser pulses at I0~ 5 1020 W/cm2, and 450 fs FWHM laser pulses at I0 ~ 5 1019 Wcm2, respectively. The inset shows the spectra obtained from a PIC simulation for a laser fluence increased by a factor of 2 and target density decreased by a factor of 2.5 with all other parameters identical to the run shown in Fig. 3.

This indication was corroborated by RCF stack data taken simultaneously to the spectral measurement with the TPs. Quantitative analysis of the RCFs indicates that the narrow band feature in the proton spectrum observed on TP1 is observed over a defined region in the RCF corresponding to a half cone beam divergence of ~ 10°. The proton spectrum gradually becomes exponential as one moves farther from the laser axis. Assuming that the divergence of the narrow band feature in the proton beam and in the carbon ion beam are comparable, the conversion efficiency into this component can be estimated as ~ 1%.
The appearance and position of the distinct peaks in the ion spectra could be controlled by varying laser and target parameters as shown in Fig. 4(a). Peaks were only observed in the limit of thin foils and high intensity, with the peaks shifting towards higher energy as either the intensity was increased or the target thickness was reduced. As shown in the Fig. 4(d), the experimental data agrees well with the ion energy estimated by a simple rigid model for RPA-LS mechanism [18,19]. As expected for the non-relativistic case, the ion energy is seen to scale as $(a_0 2\tau_p/\chi)^2$. As reported by several groups via extensive 2D and 3D simulations (see Fig. 5), the ion energy can therefore be enhanced by increasing laser fluence and/or decreasing the target areal density. However, in doing this, one needs to avoid self-induced transparency, as this terminates efficient LS (see the blue lines in the Fig. 5) and leads to a drastic reduction of the ion energy. Although the ion energies achieved here (> 10 MeV/nucleon) are encouraging, producing peaks at more than 100 MeV/nucleon would be a crucial milestone in view of applications. As shown in the insert in the Fig. 2, 2D PIC simulations predict that 100 MeV/nucleon ions in a narrow energy bandwidth can be

reached by, for example, increasing the laser fluence by a factor of 2 and decreasing the target density by a factor of 2.5, compared to the case shown in the Fig. 4(b). This seems achievable in the near term, given current developments in laser and target fabrication technology.

ACKNOWLEDGMENTS

The authors acknowledge support from EPSRC (grants EP/E035728/1 and EP/J002550/1) and from the Ministry of Education of the Czech Republic (project ECOP Nos. CZ.1.07/2.3.00/20.0279 and ELI- Beamlines CZ.1.05/1.1.00/02.0061)

REFERENCES

1. Gaillard S. A., Kluge T., Flippo K. A., Bussmann M., Gall B., Lockard T., Geissel M., Offermann D. T., Schollmeier M., Sentoku Y., and Cowan T. E., *Phys. Plasmas* **18** (5): 056710-056721, (2011)
2. Snavely R. A., Key M. H., Hatchett S. P., Cowan T. E., Roth M., Phillips T. W., Stoyer M. A., Henry E. A., Sangster T. C., Singh M. S., Wilks S. C., MacKinnon A., Offenberger A., Pennington D. M., Yasuike K., Langdon A. B., Lasinski B. F., Johnson J., Perry M. D., and Campbell E. M., *Phys. Rev. Lett*. **85** (14): 2945–2948, (2000)
3. Robson L., Simpson P. T., Clarke R. J., Ledingham K. W. D., Lindau F., Lundh O., McCanny T., Mora P., Neely D., Wahlström C.G., Zepf M. and McKenna P., *Nat. Phys*. **3** (1): 58 – 62, (2007)
4. Ogura K, Nishiuchi M, Pirozhkov AS, Tanimoto T, Sagisaka A, Esirkepov TZh, Kando M, Shizuma T, Hayakawa T, Kiriyama H, Shimomura T, Kondo S, Kanazawa S, Nakai Y, Sasao H, Sasao F, Fukuda Y, Sakaki H, Kanasaki M, Yogo A, Bulanov SV, Bolton PR, Kondo K., *Opt. Lett.* **37** (14): 2868-70, (2012).
5. B.M. Hegelich, *Bull. Am. Phys. Soc.* **56** (16): 322 (UI2.00004) (2011)
6. Zeil K, Kraft S D, Bock S, Bussmann M, Cowan T E, Kluge T, Metzkes J, Richter T, Sauerbrey R and Schramm U, *New J. Phys.* **12** (4): 045015-045032, (2010)
7. Borghesi M., Fuchs J., Bulanov S. V., MacKinnon A. J., Patel P. K., Roth M., *Fus. Sci. Techn.* **49**, (3): 412-439, (2006).
8. Macchi A., Borghesi M., Passoni A., *Rev. Mod Phys*, in press (2013), and references within
9. Borghesi M, Bigongiari A, Kar S, Macchi A, Romagnani L, Audebert P, Fuchs J, Toncian T, Willi O, Bulanov S V, Mackinnon A J and Gauthier J C, *Plasma Phys. Control Fusion*, **50,**124040-124050, (2008)
10. Wilks S. C., Langdon A. B., Cowan T. E., Roth M., Singh M., Hatchett S., Key M. H., Pennington D., MacKinnon A., and Snavely R. A., *Phys. Plasmas*, **8**,(2): 542-550, (2001)
11. Mora P., *Phys. Rev. Lett.*, **90** (18): 185002-185006, (2003)
12. Fuchs J., Antici P., d'Humières E., Lefebvre E., Borghesi M., Brambrink E., Cecchetti C. A., Kaluza M., Malka V., Manclossi M., Meyroneinc S., Mora P., Schreiber J., Toncian T., Pépin H. and Audebert P., *Nature Phys.*, **2**, 48-54, (2006)
13. Mora P., *Phys. Rev. E*, **72**,(5): 056401, (2005)
14. Schreiber J., Bell F., Grüner F., Schramm U., Geissler M., Schnürer M., Ter-Avetisyan S., Hegelich B. M., Cobble J., Brambrink E., Fuchs J., Audebert P., and Habs D., *Phys. Rev. Lett.* **97** (4): 045005, (2006)
15. Crow J.E., Auer P. and Allen J.E., *J. Plasma Phys.*, **14** (1): 65-76, (1975)
16. Passoni M. and Lontano M., *Phys. Rev. Lett.*, **101** (11): 115001-115005, (2008)
17. Passoni M., Bertagna L.and Zani A., *New Journal of Physics*, **12** (4): 045012, (2010)
18. Kar S., Kakolee K. F., Qiao B., Macchi A., Cerchez M., Doria D., Geissler M., McKenna P., Neely D., Osterholz J., Prasad R., Quinn K., Ramakrishna B., Sarri G., Willi O., Yuan X. Y., Zepf M., and Borghesi M., *Phys. Rev. Lett*, **109** (18): 185006-185011, (2012)
19. Macchi A., Veghini S, Liseykina T V and Pegoraro F, *New J. Phys.* **12** (4): 045013, (2010).